LIMNOLOGY and OCEANOGRAPHY

ASLO

Limnol. Oceanogr. 9999, 2024, 1–15

doi: 10.1002/lno.12566

Temporal evolution of plankton and particles distribution across a mesoscale front during the spring bloom

Thelma Panaïotis,[1,2*] **Antoine Poteau**,[2] **Émilie Diamond Riquier**,[3] **Camille Catalano**,[2] **Lucas Courchet**,[3] **Solène Motreuil**,[3] **Laurent Coppola**,[2,4] **Marc Picheral**,[2] **Jean-Olivier Irisson**[2]

[1]National Oceanography Centre, Southampton, United Kingdom
[2]Laboratoire d'Océanographie de Villefranche (LOV), Sorbonne Université, CNRS, Villefranche-sur-Mer, France
[3]Institut de la Mer de Villefranche, Villefranche-sur-Mer, France
[4]Sorbonne Université, CNRS, OSU STAMAR, UAR2017, Paris, France

Abstract

The effect of mesoscale features on the distribution of planktonic organisms are well documented. Yet, the interaction between these spatial features and the temporal scale, which can result in sudden increases of the planktonic biomass, is less known and not described at high resolution. A permanent mesoscale front in the Ligurian Sea (north-western Mediterranean) was repeatedly sampled between January and June 2021 using a SeaExplorer glider equipped with an Underwater Vision Profiler 6 (UVP6), a versatile in situ imager. Both plankton and particle distributions were resolved throughout the spring bloom to assess whether the front was a location of increased zooplankton concentration and whether it constrained particle distribution. Over the 5 months, the glider performed more than 5000 dives and the UVP6 collected 1.1 million images. We focused our analysis on shallow (300 m) transects, which gave a horizontal resolution of 900 m. About 13,000 images of planktonic organisms were retained. Ordination methods applied to particles and plankton concentrations revealed strong temporal variations during the bloom, with a succession of various zooplankton communities. Changes in particle abundance and size could be explained by changes in the plankton community. The front had a strong influence on particle distribution, while the signal was not as clear for plankton, probably because of the relatively small number of imaged organisms. This work confirms the need to sample both plankton and particles at fine scale to understand their interactions, a task for which automated in situ imaging is particularly adapted.

As drifters, planktonic organisms are strongly affected by the conditions of their surrounding water mass (Hays et al. 2005). Fluctuations in phytoplankton and zooplankton concentrations occur as water conditions change over time (e.g., seasons) and space (e.g., with water displacement). More specifically, strong increases in productivity and plankton concentration are referred to as "blooms" (Behrenfeld and Boss 2014). Phytoplankton blooms typically occur in temperate and polar regions at the end of winter, coinciding with the cessation of deep convection and the onset of thermal stratification, which replenishes surface water nutrients (Winder and Cloern 2010; Behrenfeld 2014). Zooplankton blooms may follow through aggregation or favorable conditions enabling an increased growth rate (Graham et al. 2001). In the latter case, the zooplankton bloom takes place slightly later than the phytoplankton bloom (Heinrich 1962). Plankton blooms also impact the concentration, composition and morphology of marine snow particles (Trudnowska et al. 2021), formed through a combination of physical coagulation and zooplankton-mediated processes (Kiørboe 2001; Burd and Jackson 2009).

*Correspondence: thelma.panaiotis@noc.ac.uk

Additional Supporting Information may be found in the online version of this article.

Authors Contribution Statement: T.P. designed the study under the supervision of La.C., M.P., and J.O.I. T.P. and A.P. piloted the glider. All authors contributed to glider deployment and retrieval. T.P., E.R., M.P., and C.C. contributed to on-land maintenance of the glider and to data transfer. C.C. developed the code for data import to EcoTaxa/EcoPart. Lu. C. and S.M. helped with sorting images. T.P. conducted the analyses and wrote the manuscript, with support from J.O.I. All authors contributed to the discussion of the results, supported manuscript preparation, and approved the final submitted manuscript.
Special Issue: Autonomous Instrumentation and Big Data: New Windows, Knowledge, and Breakthroughs in the Aquatic Sciences. *Edited by: Yui Takeshita, Heidi Sosik, Dominique Lefevre, Werner Eckert, Kevin C. Rose and Deputy Editors Julia C. Mullarney, Steeve Comeau, and Elisa Schaum.*

Physical coagulation involves particle collision due to Brownian motion, differences in sinking velocity, or fluid shear; while zooplankton-mediated processes include fecal pellets production and mucus feeding webs (e.g., Appendicularia houses). Hence, both plankton and particle distributions are affected by temporal processes, often interacting with mesoscale (∼ 10–100 km in space, ∼ 1–100 d in time) physical structures like eddies and fronts.

Physical processes operate across various scales in the oceans, from centimeters to thousands of kilometers (Legendre and Demers 1984; Dickey 1991), shaping planktonic ecosystems structure (Haury et al. 1978; Denman and Powell 1984; Legendre and Demers 1984). Fronts and eddies, in particular, play crucial roles in plankton and particles distributions (Pinca and Dallot 1995; Turner 2015). Fronts, which separate water masses with different properties, vary widely in spatiotemporal scales: from a few hundreds of meters to tens of kilometers and from ephemeral to permanent (Owen 1981; Ferrari 2011; Lévy et al. 2018). These frontal zones are oceanic hotspots of productivity and biomass across all trophic levels (Owen 1981; McClatchie et al. 2012; Lévy et al. 2018).

In a frontal-jet system, characterized by a steady geostrophic current associated with an along-current frontal structure and horizontal density gradients (Niewiadomska et al. 2008), the frontal structure can generate a submesoscale cross-frontal ageostrophic circulation directed in the sense of flattening the isopycnals (i.e., downwelling on the dense side of the front, upwelling on the light side of the front, Lévy et al. 2018). Submesoscale processes occur below the mesoscale, typically around the kilometer scale (Lévy et al. 2018). Thus, enhanced plankton biomass at the front can result either from passive organisms aggregation (Graham et al. 2001) or active mechanisms taking place after a few days, such as an increased growth rate caused by the redistribution of nutrients by the cross-frontal recirculation (Lévy et al. 2018).

This study focuses on the northern frontal-jet system of the Ligurian Sea (north-western Mediterranean). The northern current is a geostrophic jet flowing along the coast from north-west to south-east, located about 20 km offshore and stronger between the surface and 150 m, with an average speed of 30–50 cm s^{-1} (Millot 1999; Niewiadomska et al. 2008; Prieur et al. 2020). Associated with this current is a permanent mesoscale front—the Ligurian front—delimited by the 38.2 and 38.8 isohalines (Boucher 1984) and going as deep as 200 m (Niewiadomska et al. 2008). This front separates offshore colder and saltier waters from coastal warmer and fresher water, delineating three distinct zones: coastal, frontal and central (Prieur et al. 2020). The Ligurian front and jet meander between 15 and 50 km away from the coast, moving at approximately 8 km per day (Piterbarg et al. 2014). Since planktonic organisms are unable to swim against currents, their distribution should be impacted by these physical features. Resolving such mesoscale distribution of planktonic organisms and physical properties during the plankton bloom requires high-resolution spatial sampling over several months, which is not achievable with ship-based sampling. Autonomous underwater vehicles, such as gliders, can be deployed to sample continuously for weeks, resolve submesoscale hydrologic features and integrate diverse miniaturized sensors (Rudnick et al. 2004), meeting the requirements of such studies. Numerous studies have examined plankton distribution across the Ligurian frontal-jet system. Early studies highlighted the relation between the spatial distribution of planktonic organisms and the physical structure of the front (Boucher 1984; Boucher et al. 1987). More specifically, the front seems to act as a barrier, constraining organisms whether in coastal or offshore waters (Pedrotti and Fenaux 1992; Molinero et al. 2008; Faillettaz et al. 2016). The front also affected the distribution of marine snow aggregates, constraining their distribution on the coastal side of the front (Gorsky et al. 2000; Stemmann et al. 2008). Finally, regarding vertical distributions, copepod communities strongly vary between stratum (Gasser et al. 1998); and the distribution of pelagic tunicates may reflect the junction of frontal convection cells (Gorsky et al. 1991). Within the Mediterranean Sea, the Ligurian Sea is one of the locations experiencing a phytoplankton spring bloom (and occasionally, a less intense autumn bloom, D'Ortenzio and Ribera d'Alcalà 2009; Mayot et al. 2017; Mayot et al. 2020), which subsequently propagates to higher trophic levels, resulting in increased concentrations of zooplankton such as copepods (Dolan and Raybaud 2020) or salps (Nival et al. 2020).

Evidence suggests that phytoplankton blooms are influenced by the previously described frontal features. Goffart et al. (1995) observed a more intense bloom at the front, with phytoplankton transported downward by the frontal convergence following the isopycnals. As described above, submesoscale frontal features can influence phytoplankton distribution and growth (Lévy et al. 2018). Glider surveys of the Ligurian front detected vertical transport of surface waters enriched in chlorophyll, highlighting such effect (Niewiadomska et al. 2008). Investigating how these effects propagate to higher trophic levels (e.g., zooplankton, larval fish) thus requires studying their distribution at the same resolution as phytoplankton. This fine-scale resolution captures interactions between planktonic organisms, as well as interactions with their physicochemical environment. Several studies already targeted zooplankton distribution at such scales: Luo et al. (2014) showed that the distribution of various gelatinous organisms across a mesoscale front was driven by temperature, depth, oxygen, or chlorophyll *a* (Chl *a*) concentration depending on the taxonomic group. Similarly, Greer et al. (2015) showed increased abundance of both zooplankton and larval fish on the shelf side of a shelf-slope front. Finally, Greer et al. (2013) revealed the interaction between phytoplankton fine layers and zooplanktonic grazers. The common denominator between these studies is that they rely on in situ imaging.

Traditional plankton sampling instruments (nets and pumps) are inadequate for resolving the fine-scale distribution of planktonic organisms in relation to their immediate environment. They lack spatiotemporal resolution because they

integrate organisms over tow distance and/or depth. Furthermore, plankton sampling is often performed separately from environmental data recording (Cowen and Guigand 2008; Lombard et al. 2019). In addition, fragile organisms can be damaged during sampling, resulting in underestimated concentrations (Remsen et al. 2004). The development of in situ imaging instruments overcame some of these limitations: they resolve the fine-scale distribution of planktonic organisms within their environment and allow the detection of physico-biological relationships, while preserving organisms and enabling in situ behavior observation (Mars Brisbin et al. 2020; Orenstein et al. 2021; Vilgrain et al. 2021). However, this comes at the cost of some taxonomic resolution and of a large data processing effort. The Underwater Vision Profiler 6 (UVP6) (Picheral et al. 2021) is one of these in situ imagers, targeting mostly zooplankton and large phytoplankton colonies. Compared to the previous generation (UVP5) (Picheral et al. 2010), the UVP6 is smaller and can be deployed on autonomous platforms (e.g., float, glider).

In this work, we leverage in situ imaging collected by a glider to tackle the following questions: what are the physical and biological properties of the Ligurian front; what are the dynamics of particles and plankton distribution across the front during the spring bloom of 2021?

Materials and methods

Glider and UVP6

Sampling was performed with a Seaexplorer (Alseamar) glider, an autonomous underwater vehicle taking advantage of buoyancy variations to glide forward through the water in a sawtooth-like pattern, surfacing periodically to ensure data transmission and GPS positioning. The glider was fitted with a set of sensors to record temperature, salinity, fluorescence, particles backscattering at 700 nm (BB700), color dissolved organic matter (CDOM) and dissolved oxygen concentration. The glider was also equipped with a UVP6-LP, consisting of a main camera and a light unit illuminating a slice of water for an image volume of 0.67 liter, with an adaptable imaging rate of up to 1.3 Hz (Picheral et al. 2021). With a pixel size of 73 μm, it captures images of plankton and marine snow above 600 μm and counts particles above 80 μm in equivalent spherical diameter (ESD). When embedded on a Seaexplorer glider, the UVP6-LP is deployed in supervised mode and is controlled by the glider using a preset configuration (out of 10 possible), with the ability to update settings remotely. While the UVP6 operated both during downcasts and upcasts, sunlight interference is possible below the surface during daily and very sunny upcasts. To mitigate this, black images were regularly recorded to identify increased noise levels caused by sunlight. Images acquired in such conditions were discarded, resulting in the absence of data above ~40 m during daytime upcasts. Finally, depth-averaged current was estimated using navigation data from the glider: by comparing its estimated position with GPS fixes upon surfacing, any deviation was attributed to the depth-averaged current affecting the glider navigation.

Mission design

The glider was deployed outside of Villefranche Bay (43°39′18″N, 7°17′24″E, referred as to "coast"), heading towards the Dyfamed point (43°22′02″N, 7°55′59″E). Sampling consisted of repeated transects, crossing nearly perpendicularly the Ligurian front. The glider performed round-trips between the coast and Dyfamed, conduction 10 missions from before (28 January 2021) to after (28 June 2021) the spring bloom (Fig. 1). Each mission (12–14 d each) consisting of two round trips from the coast. During outbound journeys, the glider's trajectory slightly adjusted into the current and it dove down to 600 m to avoid the strong surface (< 150 m depth) jet. On return trips, the target depth was reduced to 300 m to increase horizontal resolution, with a median distance of 900 m between surfacing events. The UVP6 acquisition rate was set to 0.2 Hz below 220 m and to 0.5 Hz above (1.3 Hz for the last two missions), resulting in a sampling rate between

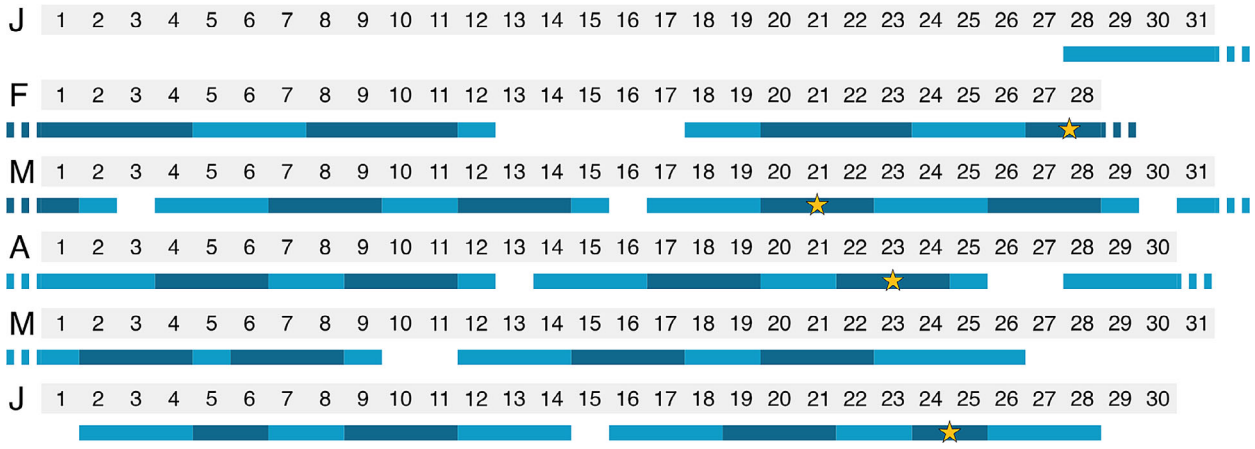

Fig. 1. Schedule of the 10 glider missions. Each mission consisted of 2 round trips; darker parts represent back transects on which we focused our analysis. Stars show transects selected for a synthetic visualization in the rest of the paper.

0.14 and 0.91 L s^{-1}. During the 10 missions, the glider spent 2790 h at sea, the UVP6 capturing a total of 1,123,123 images. However, 30% of these images were captured near the coast when the glider was in virtual mooring (i.e., performing dives but staying in a designated location, heading against the current) before recovery.

Data processing

Positional data

First, each transect was separated into "out" and "back" parts based on surfacing position and only back parts (with higher horizontal resolution) were retained. The resolution of "out" parts of transects (~ 2 km between surfacing events) was too low to investigate the effects of the front on plankton distribution. This resulted in a total of 20 transects (Fig. 1). As each transect lasted more than 24 h, it is not always possible to clearly determine whether a given signal is due to space (e.g., frontal zone) or time (e.g., daytime vs. nighttime). GPS positioning being available only when the glider was surfacing, geographical coordinates were linearly interpolated during dives, each consisting of a down and an upcast. Latitude and longitude were then used to compute the distance from shore (reference point at Nice cape, 43°41′9″N, 7°18′17″E).

Plankton images

Images captured by the UVP6 during cruising (n = 785,405) were first imported into the Morphocluster application (Schröder et al. 2020) to quickly detect large clusters of similar objects. This allowed sorting more than 400,000 objects, mostly detritus, in a few hours. In a 2nd step, images collected during back transects (the focus of this study, n = 434,129), were imported onto the EcoTaxa web application (Picheral et al. 2017) with their Morphocluster label in order to be sorted into finer taxonomic or morphological groups (marine snow, artifact, badfocus, reflection, or unidentifiable) with the help of supervised machine learning. Still, sorting all 400k+ images would have required a multiple-month effort and we instead decided to rely on the predictions of a Random Forest (RF) classifier fed with both handcrafted and deep (i.e., generated by the feature extractor part of a convolutional neural network [CNN]) features generated by a MobileNet V2 (Sandler et al. 2019) feature extractor previously finetuned on UVP6 data. We selected a RF classifier because they tend to produce good classification probability estimates (Niculescu-Mizil and Caruana 2005), are faster to train than a full CNN stack and perform as well as a full CNN when trained with deep features (E. Amblard pers. comm.).

Classification performance was assessed on an independent test set (n = 42,595) not used for training. This test set was built to be representative of the whole dataset by selecting 1 out of 10 profiles, equally distributed across the mission. Unsurprisingly, the test set was dominated by detritus (n > 40,000) but still contained around 100 objects or more per category for a few taxonomic groups (Copepoda, Appendicularia, Rhizaria, Salpida), allowing to compute reliable classification performance metrics. This revealed relatively poor precision performance for a few groups, including Appendicularia and Rhizaria (Supporting Information Table S2). To improve precision, at the expense of recall, and ensure that observed patterns were genuine, we applied a probability threshold (Faillettaz et al. 2016) on classification scores. This threshold, set independently for each class, ensured that objects predicted in a given class with a score above the threshold actually belonged to this class for at least 75% of them (i.e., targeting a precision of 75%, Supporting Information Table S3), discarding images with a prediction score below the threshold. However, this approach strongly decreased recall for Appendicularia and Rhizaria, impeding the detection of any distribution pattern. Consequently, the probability threshold was not applied to these classes, that were instead fully inspected and manually validated (n = 1500), resulting in 100% precision (all objects assigned to one of these classes do belong to the assigned class) without decreasing recall. Counts of objects per taxonomic group and per particle size class were divided by water volumes sampled to compute concentrations (# m^{-3}) within 5 m bins along the glider trajectory.

Environmental data

First, abnormal values (e.g., negative fluorescence) were discarded. Density was computed from temperature and salinity using the "gsw" R package version 1.1.1. For each variable, outliers were detected according to deviation around the median (Leys et al. 2013) and removed. Oxygen concentrations were adjusted by subtracting a 52 μmol kg^{-1} offset, derived from comparisons with values recorded simultaneously at Dyfamed. Data were linearly interpolated at 1 m resolution to fill in missing values. Each variable was smoothed using a moving average within a window size of 25 m. Data were then binned over 5 m to match the plankton and particles data bins.

Data analysis

Particles

First, particle concentrations for 13 size classes between 102 μm (the 1st class entirely above the detection threshold of 80 μm) and 2.05 mm (larger classes contained too few particles and were thus noisy) were averaged onto 10 m × 1 km bins to reduce noise and normalized with log-transformation to avoid very high values. A principal component analysis (PCA) was then performed to summarize these concentrations, scaled to unit variance so that each size class equally contributed to the construction of the factorial space. Supplementary variables (biogeochemical variables and metadata)—not used to compute the PCA space—were projected onto the PCA space to help with the interpretation. Finally, scores of objects were visualized on transects.

Plankton

A PCA was also performed to synthesize plankton concentrations. Because of the scarcity of the plankton compared to the > 80 μm particles, plankton concentrations were first averaged across 30 m × 5 km bins, resulting in a median water volume of 373 liters ($Q1$ = 183 liters, $Q3$ = 573 liters) per bin.

Still, many bins lacked plankton, resulting in a zero-inflated distribution. To address this, only bins where plankton was present were considered, and the average value for each variable (i.e., concentrations of plankton groups) was assigned to empty bins to ensure they did not distort PCA space. All concentrations were $\log(n+1)$-transformed to normalize them and standardized by subtracting the mean and dividing by the standard deviation (Legendre and Legendre 2012), so that each taxon contributed equally to the construction of the PCA space.

This PCA (Supporting Information Fig. S8) highlighted the importance of a few taxonomic groups: Copepoda and Eumalacostraca emerged on PC1, Salpida, Mollusca and Appendicularia on PC2, and multiple Rhizaria subgroups on PC3. We decided to focus our analyses on four groups based on their abundance (Supporting Information Fig. S7) and their importance in the PCA: Copepoda, Appendicularia, Salpida, and Rhizaria other than Collodaria and Foraminifera (since this group of other Rhizaria taxa was the most abundant and was representative of all three Rhizaria groups, since they had close projections in the PCA space).

Visualization

Four transect representatives of the dynamics of the bloom (Fig. 1) were chosen from the available 20 to offer a condensed view in the main manuscript. However, supplementary material includes all 20 transects (Supporting Information Fig. S1, S5, S8, S9, and S10).

All analyses were conducted with R version 4.1.2. Data processing and interpolations were performed with packages dplyr and akima, respectively. Plots were generated with ggplot2 using the color-blind friendly viridis and cmocean color scales.

Results

Dataset composition

During the back transects, the UVP6 imaged 434,129, of which 305,294 were confidently predicted and retained after probability thresholding. After discarding marine snow particles, imaging artifacts and unidentifiable objects, 12,824 images of planktonic organisms, sorted into 10 taxonomic groups, were retained. Copepods dominated the dataset, followed by Rhizaria, Appendicularia, and Salpida (Supporting Information Fig. S7).

Environment

Transect maps (Fig. 2) show that the Ligurian current was stronger in late winter and early spring, and weakened later in the spring. Although globally oriented NE to SW, changes in current direction on 20 March 2021 (top-left panel in Fig. 2) highlights the presence of a meander.

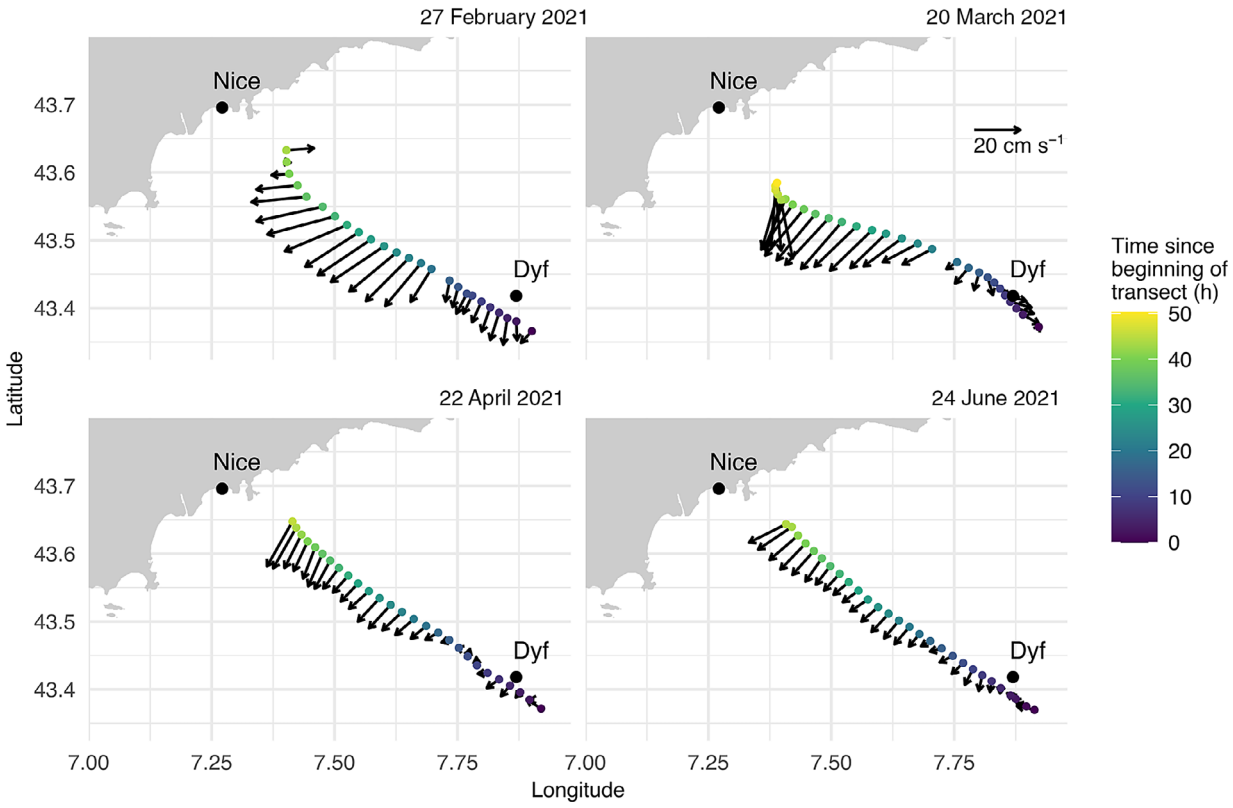

Fig. 2. Map of four representative transects, showing depth-averaged current across the water column. Transects started around the Dyfamed point and aimed toward Nice. Dyf = Dyfamed.

The first presented transect (starting on 27 February) revealed a rather homogeneous temperature over the water column (Fig. 3; Supporting Information Fig. S1). At the surface, the front was located between 20 and 30 km offshore, and separated fresher waters inshore from saltier waters offshore, as expected. Fluorescence highlighted an intense bloom at the surface in offshore waters. Chlorophyll-enriched water was detected down to 300 m, well below the photic zone, thus corresponding

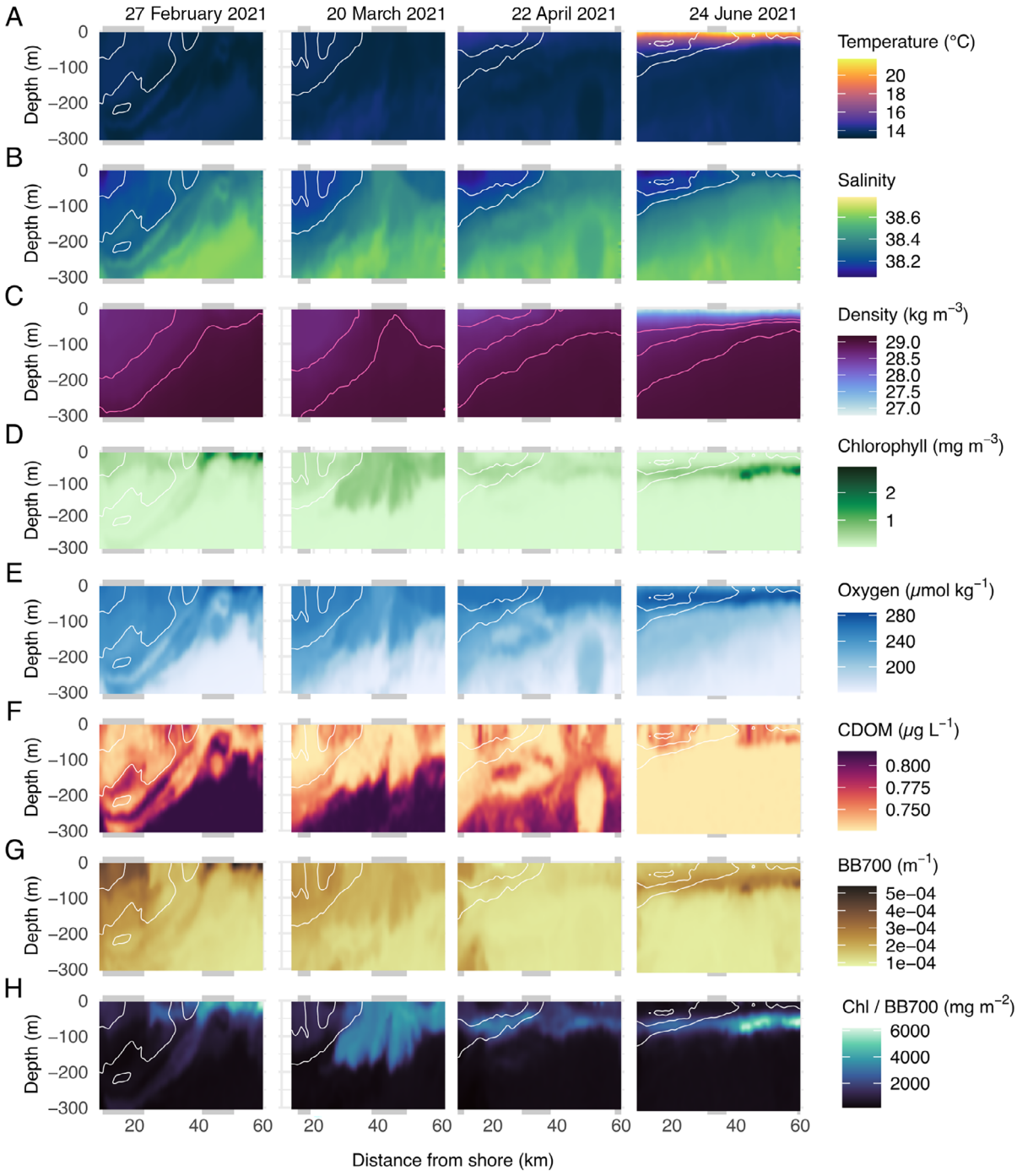

Fig. 3. Evolution of environmental conditions across four transects representative of the dynamics during the bloom. Each column is labeled according to the starting date of the transect, which began offshore, on the right. Each transect lasted about 2 d and gray rectangles in the plot background represent night time. (**A**) Temperature; (**B**) salinity with the 38.2 and 38.3 isohalines delimiting the front; (**C**) potential density anomaly with the 28.6, 28.8, and 29 isopycnals; (**D**) chlorophyll; (**E**) oxygen; (**F**) CDOM; (**G**) BB700; and (**H**) chlorophyll to BB700 ratio. Plots for all transects are presented in Supporting Information Fig. S1.

to a downwelling of water enriched in chlorophyll that seemed to follow the front. This feature was also clearly visible on salinity, oxygen and CDOM, strongly suggesting a movement of a whole water mass. Finally, inshore waters were well oxygenated down to 300 m. The 2nd transect (20 March) displayed similar features except for fluorescence: an important mixing event was detected, down to 200 m, where no photosynthesis can take place. This event was also visible on oxygen and CDOM concentrations. This mixing event was likely caused by strong winds the day before (Supporting Information Fig. S3). On the 3rd transect (22 April), a weak stratification appeared in coastal waters and the 38.2 and 38.3 isohalines delimiting the front became more horizontal. Fluorescence was lower at the very surface than in the waters below, hinting at the formation of a deep chlorophyll maximum (DCM). A lens of colder and fresher water was located 50 km offshore, between 150 and 300 m depth, and was also characterized by higher oxygen and lower CDOM. Finally, on 24 June, the water column was well stratified, with sharp thermocline and pycnocline. The isohalines, and thus the front, were nearly horizontal. The DCM was well established between 50 and 100 m (also visible on BB700), with higher chlorophyll concentration and higher chlorophyll to BB700 ratio offshore, indicating a higher concentration of phytoplankton cells. Oxygenated waters were restricted to the surface, above the DCM. These features are emblematic of the oligotrophic environment during summer in the Ligurian Sea.

Particles distribution

For particles, the first two axes of the PCA captured 83.9% of variance, most of it (60.2%) being on the 1st axis (Fig. 4A). This axis separated high particle concentrations, associated with coastal waters characterized by high BB700, oxygen and fluorescence, from low particle concentrations, associated with offshore, deep, salty, and dense waters. The 2nd axis discriminated between size classes. PC1 projections (Fig. 4B) highlighted a decrease in particle concentration decrease over time, while PC2 projections (Fig. 4C) revealed contrasted patterns in particle size. On 27 February and 20 March, coastal areas exhibited greater particles abundance, with larger particles correlating with the downwelling event detected on fluorescence (Fig. 3). Particles were larger offshore than inshore (Fig. 4C). On 22 April, particle concentration was much lower, except in very coastal waters, highlighting the near absence of particle export. Large particles were present in the 0–100 m depth layer, around the forming DCM, but not below. Finally, on 24 June, the DCM was associated with abundant small particles, likely phytoplankton cells or particles produced through biological activity; while a rain of larger particles was detected offshore, below the DCM. The circadian cycle did not seem to affect neither particle distribution nor size in any transect.

Plankton distribution

Concentration plots for the selected taxa highlighted changes in the zooplankton community (Fig. 5; Supporting Information Fig. S10). Copepods and appendicularians dominated close to the surface in February, especially offshore. In March, copepod abundance intensified, while appendicularians declined, replaced by salps at the top of the water column on the offshore side of the front. A 2nd peak in Appendicularia abundance occurred in April, while salps were still present. In June, rhizarians became more abundant in the entire water column while copepods, appendicularians and salps were less abundant. Finally, at the considered scale, no effect of the circadian cycle could be detected.

Discussion

Plankton and sampled volumes

Due to the low sampling rate (≤ 0.9 L s^{-1}), very few planktonic organisms were imaged, with just 13,000 being confidently predicted for analysis. Thus, many sampled bins lacked, resulting in a weaker signal compared to particles data. Overall, only 17,000 objects were predicted as plankton, such that manual validation of all plankton groups would have only added 4000 organisms (+30%), likely not affecting our results. Still, we cannot exclude that planktonic organisms were predicted as detritus, necessitating the inspection of > 400,000 images. Despite an increased sampling rate towards the end of the mission (from 0.35 to 0.91 L s^{-1}, the maximum achievable for the UVP6-LP) in the 0–220-m layer, this was still insufficient to investigate fine scale plankton distribution. To resolve such scales, the UVP6-LP would need to be run at its highest rate of 1.3 Hz instead of 0.2 and 0.5 Hz during this experiment (the last two deployments were indeed run at a sampling rate of 1.3 Hz); or a UVP6-HF (high frequency, Picheral et al. 2021) capable of sampling at 20 Hz, albeit with higher energy consumption and reduced glider autonomy (e.g., only one round-trip per deployment). Still, our work confirms the effectiveness of autonomous underwater vehicle such as glider fitted with in situ imager to sample both the environment, particles and plankton at fine scale over extended durations. Nonetheless, as mentioned above, attention to sampling resolution, particularly that of the imager, is crucial for achieving research objectives.

However, it should be noted that our study area, being oligotrophic, has relatively low concentrations of the planktonic organisms targeted by the UVP6. For instance, the expected average concentration for *Centropages typicus*, a very common, large (~ 1 mm) copepod of the Ligurian Sea (Dolan and Raybaud 2020), is about 30 ind m^{-3}, while the UVP6 sampling rate was ~ 0.9 L s^{-1} (or ~ 20 min m^{-3}). While insufficient to resolve fine-scale plankton distribution in such oligotrophic conditions, this sampling rate could have been adequate in richer areas.

Challenges posed by temporal and spatial variabilities

Overall, the data collected by the glider consist of repeated ~ 50 km transects over several months. However, these

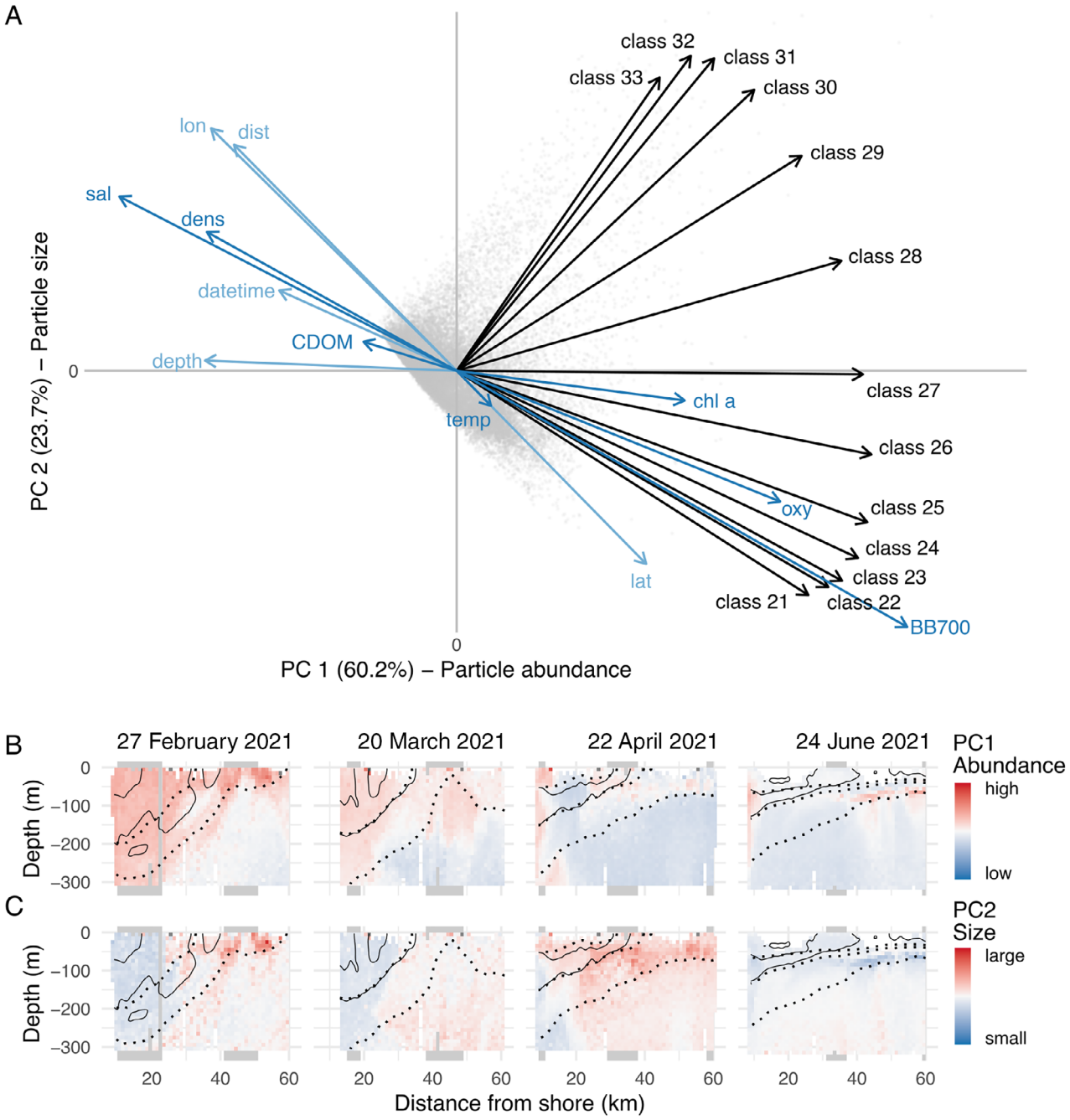

Fig. 4. Evolution of particles distribution. (**A**) PCA performed on log-transformed particle concentrations. Definition of size classes: Class 21: 102–128 μm, Class 22: 128–161 μm, Class 23: 161–203 μm, Class 24: 203–256 μm, Class 25: 256–323 μm, Class 26: 323–406 μm, Class 27: 406–512 μm, Class 28: 512–645 μm, Class 29: 645–813 μm, Class 30: 813–1020 μm, Class 31: 1020–1290 μm, Class 32: 1290–1630 μm, Class 33: 1630–2050 μm. Maps of the projections of bin scores on PC1 (**B**) and PC2 (**C**), for the four representative transects. The 38.2 and 38.3 isohalines delimiting the front are represented as continuous black lines; the 28.6, 28.8, 29 isopycnals are represented as dotted black lines. Gray rectangles in the plot background represent night time. PC1 and PC2 projections for all transects are presented in Supporting Information Fig. S5.

transects, averaging 51 h, do not always allow clear differentiation between spatial and temporal features, for example, whether a signal is caused by the diel cycle or by location relative to the front. To detect purely spatial effects, transects should be sampled as snapshots, as permitted by towed instruments such as the In Situ Ichthyoplankton Imaging System (ISIIS) (Cowen and Guigand 2008), which can cover several dozen kilometers in a few hours. Furthermore, such

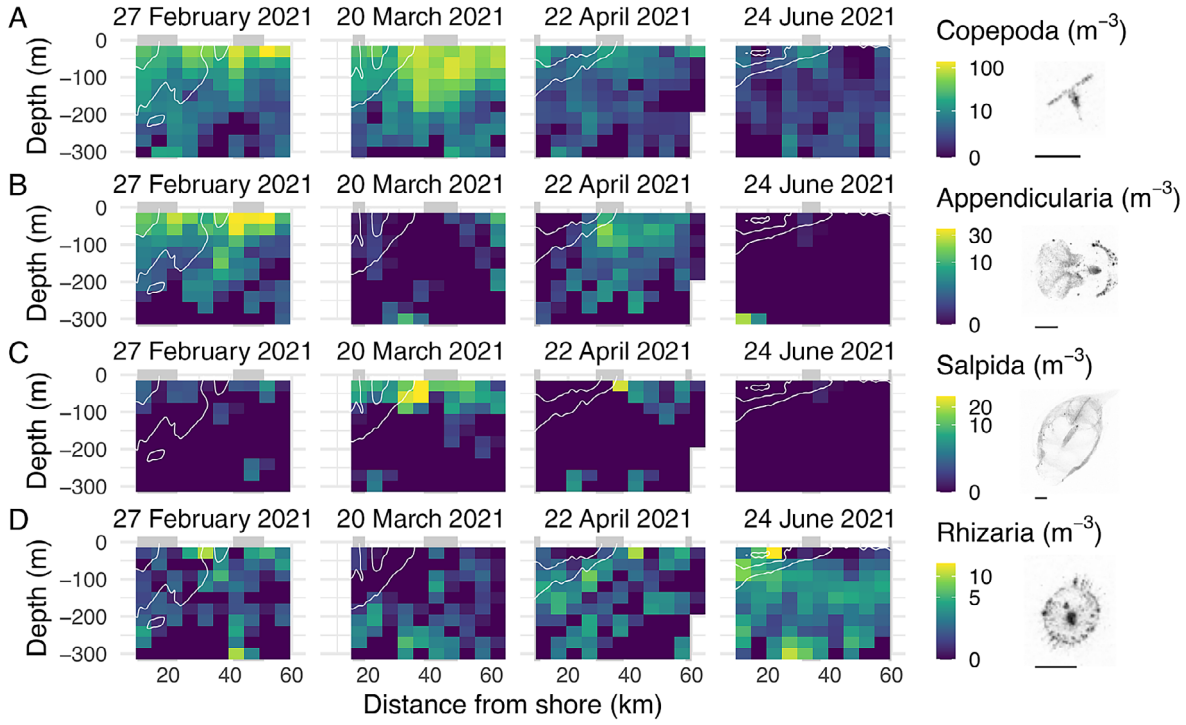

Fig. 5. Evolution of plankton distribution for the four selected groups: (**A**) Copepoda, (**B**) Appendicularia, (**C**) Salpida, and (**D**) Rhizaria. The 38.2 and 38.3 isohalines delimiting the front are represented as black lines. Gray rectangles in the plot background represent night time. Note that color scales are log-transformed and different for each taxon. Scale bars represent 2 mm. All transects are presented in Supporting Information Fig. S9.

instruments are little affected by water movement, whereas gliders can be strongly affected by currents, leading us to reconsider our original sampling strategy of sampling 0–200 m during backward transects. However, continuous sampling for 5 months is not feasible with a towed instrument, while gliders offer reasonable human costs. Conversely, for purely temporal effects, fixed-positions timeseries are required. Glider sampling lies between these two extremes views (space vs time), offering better spatial resolution than timeseries but falling short of snapshot transects' spatial resolution. Nevertheless, repeated transects offer temporal insight of observed features, which is much more difficult with single-transect approaches (Niewiadomska et al. 2008). External clues also aid interpretation (e.g., relating the downwelling observed on 20 March to preceding wind event).

Moreover, spatial features also evolve temporally: the intensity of the Ligurian current varies seasonally (more intense in winter) while meandering induces variability (Millot 1999). Finally, another difficulty arises from the short-lived nature (usually < 1 d) of targeted submesoscale features. Although we detect two submesoscale coherent vortices (SCV, discussed below), including one that was sampled twice, such events are sporadic, likely missing many other opportunities. The same goes for plankton and particle distribution, we did capture some spatial and temporal features but presumably missed many others.

Effects of the diel cycle

Space and time variations could not be disentangled. However, the PC projections did not seem affected by day/night variations, indicating little influence from the diel cycle. Two tests were performed to assess this hypothesis. First, average plankton concentrations along glider yos were computed, and differences between day and night yos were investigated with a Wilcoxon test. This highlighted day/night differences in average concentration over 0–300 m for several taxa (Supporting Information Fig. S11A). Then, average vertical distributions on 30-m bins were computed for day and night and compared with a Kolmogorov–Smirnov test, revealing significant differences for Foraminifera only (Supporting Information Fig. S11B). The UVP6 (former version of the sensor) being dazzled by the sunlight in the upper part of the water column (depth < 40 m) when ascending, no concentration of particle or plankton were computed in this zone. As no data are available to compare with night values at these depths, even though many taxa are known to migrate within this depth range, we tested the relative effect of both environmental variables and a binary day/night variable on plankton concentration in the 30–60 m depth range, using a nonlinear model (Boosted Regression Trees). For each of the four taxa, the day/night effect explained less than 8% of total variance. Overall, the little effect of the diel cycle on plankton distributions likely results from the low number of detected organisms and the averaging across relatively large bins.

Dynamics of plankton and particles during the bloom

Surface Chl *a* data in the area covered by the glider show a sudden increase on 23 February (Supporting Information Fig. S2), likely corresponding to the beginning of the phytoplankton bloom. UVP6 data indicate that the zooplankton bloom began somewhere between 20 February and 27 February, although precision is limited by our data, but the zooplankton bloom typically following the phytoplankton bloom, the latter part of this interval is more likely. Nonetheless, a physical aggregation of zooplankton could have occurred earlier than the start of the "true" bloom, that is, increased growth rate. As described below, variations observed in particle abundance and size seems to indicate that particulate organic carbon (POC) export was affected by the composition of the plankton community, as previously reported by numerous studies (Boyd and Newton 1995, 1999; Guidi et al. 2009, 2016). Indeed, zooplanktonic organisms are directly involved in POC production (Turner 2015; Steinberg and Landry 2017). Four phases emerged from the analysis particle and plankton distribution and are discussed below.

Early bloom—February

In February, the early phase of the zooplankton bloom was characterized by the presence of Appendicularia, including both inhabited and discarded houses, mostly in the 0–200-m layer. Appendicularia—filter-feeding pelagic tunicates—grow a mucopolysaccharides and cellulose house used as an external mucous filter to collect food particles (Alldredge and Madin 1982). The house is disposable: when filters obstruct, it is discarded and renewed (up to several times a day, Sato et al. 2003), contributing significantly to marine snow aggregates (Alldredge and Silver 1988). These large (3 mm ESD on average) particles have a relatively low sinking velocity (20–50 m d^{-1}) during the 1st hour, which then increases to 100 m per day after their initial deflation (Lombard and Kiørboe 2010). High Appendicularia abundance was previously linked to increased export of large particles, mostly through discarded houses (Alldredge et al. 2005). Thus, the displacement event of large particles, along the isopycnals (Fig. 3) could correspond to these discarded houses, or fecal pellets, from Appendicularia.

Mid bloom—March

In a 2nd phase, copepods dominated the 0–200-m layer while salps occupied the 0–100-m layer. Large particles, though fewer than in February, were primarily offshore. Strong wind was recorded a few days before this transect (Supporting Information Fig. S3), causing a mixing of the water column and a redistribution of phytoplankton (likely responsible for the lower Chl *a* concentration than in February, through dilution effect), particles (Figs. 1DG, 3BC) and possibly zooplankton (see pattern of copepods in Fig. 4A). Such events have previously been reported during spring and can result in community changes both for phytoplankton (Thyssen et al. 2014) and zooplankton (Romagnan et al. 2015).

Late bloom—April

In April, the concentration of appendicularians increased, while that of copepods decreased. This gelatinous bloom could be the result of favorable conditions following the wind gust 2 weeks earlier (20 March), aligning with findings by Ménard et al. (1994) who found that wind promoted blooms of salps, although this result could not be confirmed by Licandro et al. (2006). Concurrently, stratification began in coastal waters and the DCM started to form. The water column was mostly depleted in particles (except for very coastal waters). Particles present in the 0–100-m layer were rather big, a result of a decline in small particles concentration (Supporting Information Fig. S6). Further analyses showed that only 10% of objects in the 1–2 mm size range were living organisms, confirming that these large objects are indeed particles and not planktonic organisms such as appendicularians, more abundant in the same depth range. These large particles, distributed along the isopycnals, raised questions regarding particle dynamics. A 1st hypothesis could be a lack of aggregation, so that organic matter would remain in the form of small particles (< 80 μm) undetected by the UVP6. However, backscattering measurements (targeting particles around 10 μm), also show low abundance in the water column on 22 April 22 (Fig. 2; Supporting Information Fig. S1), challenging this explanation. Alternatively, the decrease in small particles might be caused filter-feeding tunicates such as salps and appendicularians in the water column. Both taxa contribute to particles (1 μm to 1 mm) removal (Alldredge and Madin 1982) and aggregation into larger sinking particles, explaining the relative dominance of large particles. While fecal pellets produced by salps are relatively large (~ 5 mm) and fast sinking (~ 2000 m d^{-1}, Bruland and Silver 1981), recently discarded houses of appendicularians (containing fecal pellets) sink very slowly (< 50 m d^{-1}, Lombard and Kiørboe 2010). These particles are thus much likely to reside in the water column, by sitting on density gradients.

After bloom—June

Finally, both stratification and DCM intensified while zooplankton concentration decreased (Fig. 2). Rhizaria dominated the zooplankton community, with some of them being mixotrophic and typical of oligotrophic environments (Biard et al. 2016). We mostly detected small unidentifiable Rhizaria and solitary Collodaria. The analysis of a time series of the complete plankton assemblage from net samples collected in Villefranche Bay highlighted a peak of Rhizaria in July (Romagnan et al. 2015), in oligotrophic conditions that are comparable with our transect at the end of June. The fine-scale distribution of these organisms during the oligotrophic summer was previously studied across the Ligurian front, using the ISIIS, an in situ imager with very high sampling rate (> 100 L s^{-1}) (Cowen and Guigand 2008). Solitary Collodaria

precisely followed the DCM, while Acantharia were mostly found on the coastal side in the upper 50 m of the water column (Faillettaz et al. 2016). Such patterns could not be resolved with the UVP6, mostly because of its lower sampling rate (< 1 L s^{-1}), which required to aggregate observations into broader taxonomic groups and onto a much coarser spatial grid. Particle distribution revealed more abundant and smaller particles around the DCM, which could correspond to large phytoplanktonic cells (> 100 μm) or the accumulation of particles related to biological activity.

Mesoscale features

Particles

Previous studies reported a strong influence of the front on the distribution of particles with small aggregates being more abundant in coastal waters while large aggregates were more abundant in the frontal zone, likely formed through physical coagulation or biological transformation (Gorsky et al. 2002; Stemmann et al. 2008). Moreover, large particles being more abundant in surface waters suggests local formation before downward export (Stemmann et al. 2002). Our study corroborates these findings, with small aggregates more abundant in coastal waters and the front acting as a barrier to particles spreading offshore, a consistent pattern throughout the blooming phase. Furthermore, mean aggregate concentrations (0.75 L^{-1} in 512 μm to 1.02 mm; 0.09 L^{-1} in 1.02–2.05 mm) closely matched previous observations (Stemmann et al. 2002). However, while large aggregates were sometimes more abundant under the frontal zone, this was not consistently observed (Supporting Information Fig. S5).

Plankton

Many studies detected an effect of the front on planktonic organisms distribution, either an increase in abundance or biomass at the front (Boucher 1984; Boucher et al. 1987; Molinero et al. 2008; Licandro and Icardi 2009) or different concentrations of certain taxa on either side of the front (Pedrotti and Fenaux 1992; Molinero et al. 2008; Faillettaz et al. 2016). Such effects were less evident in our data. First, the coarse spatial resolution imposed by the UVP6-LP sampling rate made it difficult to identify processes "at the front." As mentioned above, the use of a UVP6-HF with a higher sampling rate could have enhanced the detection of front-related effects on plankton distribution. Second, the coarse taxonomic resolution may have hidden some underlying differences within broad taxonomic groups (e.g., copepods). Finally, the proximity of the current to the coast for most of the study period resulted in limited sampling of coastal communities, making them difficult to contrast with offshore ones. Still, the concentration of several taxa was higher in the offshore region than in the current or in the coastal one: copepods in February and March, appendicularians in February and April, salps in March and April (Fig. 4), which is compatible with a potential barrier effect of the front.

Fine-scale features

Submesoscale coherent vortices

During the back transect on 22 April, a SCV (referred hereafter as L3) was identified. Spanning 9 km × 200 m, located between 46 and 55 km offshore and at depths from 130 to ~ 300 m, it consisted of cold, freshwater with high oxygen and low CDOM concentrations, but was barely visible on density and BB700 (Fig. 3). Similar structures were looked for in the whole dataset, including outgoing transects. The same structure, albeit smaller (5 km width, labeled L2 in Supporting Information Fig. S4), was crossed 17 h earlier on the outgoing transect on 20 April. Another similar structure (L1), closer to the coast, was detected on the same outgoing transect but not captured before during the previous back transect, performed 25 h before. This provides insight into its drift speed, estimated at 5–10 cm s^{-1}, assuming the same dimension in x and y axes. Previous detection of SCV in the area (Bosse et al. 2017) highlighted differences in physico-biogeochemical properties (more oxygen, less nutrients) compared to surrounding waters, affecting the phytoplankton community and highlighting reduced lateral exchanges between the core of the SCV and the surroundings (Bosse et al. 2017). However, no significant effect of the SCV on particle concentration or size was detected (Supporting Information Fig. S5), suggesting a limited barrier effect for particles. While changes in the phytoplankton community inside the SCV are likely to propagate to zooplankton, the sampling resolution of planktonic organisms was insufficient to detect such effects.

Subducting water mass

On 27 February, a water mass with high chlorophyll, high oxygen, low salinity, low temperature and low CDOM was recorded down to a depth of 300 m (Fig. 2; Supporting Information S1). This layer, about 3.8 km in width and 20 m in height, was sinking toward the coast, following the isopycnals along the front. This is coherent with a convergence event (Boucher et al. 1987) and was already observed by Niewiadomska et al. (2008) from glider data collected on a similar transect across the Ligurian front in January. They detected a similar water mass, 4 km wide, subducting to 180 m depth. Analogous features were reported during spring in the Corsican side of the Ligurian current: phytoplankton produced in the surface layer was carried downward along the isopycnals, forming a plume of chlorophyll down to 100 m (Goffart et al. 1995). Here, we additionally demonstrate that this instability-driven sinking water mass also carried more and bigger particles from the surface toward the depth, while it was previously only suggested that particles could be transported downward by the frontal circulation along the isopycnals (Gorsky et al. 1991).

Conclusion

In conclusion, repeated sections across the Ligurian front conducted with a glider allowed us to resolve submesoscale

hydrological features. A clear link emerged between the environment, the distribution of particles and, to some extent, that of planktonic organisms, for example, in a subducting water mass and during a mixing event. Moreover, the accumulation along isopycnals creates the DCM in April and July, reflected in the distribution of particles. Strong changes were detected in plankton distribution during the blooming period, with a succession of different zooplankton communities throughout the bloom. These changes were also related to changes in the abundance and size of marine snow particles. Although the front exhibited a consistent influence on marine snow particle distribution throughout the sampling period, the signal was coarser for planktonic organisms, probably due to the low sampling rate, resulting in a limited number of imaged organisms. Overall, these results confirm the need to study physics, biogeochemistry and biology at the same scale, by sampling both the environment, particles and plankton at fine scale using in situ imaging. This approach should allow to better understand the biological responses to submesoscale hydrological forcings.

Data availability statement

Data supporting this study is available on SEANOE: https://doi.org/10.17882/95806. Code to perform data processing and analyses is made available at https://github.com/ThelmaPana/glider_uvp6.

References

Alldredge, A. L., and L. P. Madin. 1982. Pelagic tunicates: Unique herbivores in the marine plankton. Bioscience **32**: 655–663. doi:10.2307/1308815

Alldredge, A. L., and M. W. Silver. 1988. Characteristics, dynamics and significance of marine snow. Prog. Oceanogr. **20**: 41–82. doi:10.1016/0079-6611(88)90053-5

Alldredge, A. 2005. The contribution of discarded appendicularian houses to the flux of particulate organic carbon from oceanic surface waters, p. 315–332. In G. Gorsky, M. J. Youngbluth, and D. Deibel [eds.], Response of marine ecosystems to global change: Ecological impact of appendicularians. Archives Contemporaines.

Behrenfeld, M. J. 2014. Climate-mediated dance of the plankton. Nat. Clim. Change **4**: 880–887. doi:10.1038/nclimate2349

Behrenfeld, M. J., and E. S. Boss. 2014. Resurrecting the ecological underpinnings of ocean plankton blooms. Ann. Rev. Mar. Sci. **6**: 167–194. doi:10.1146/annurev-marine-052913-021325

Biard, T., and others. 2016. In situ imaging reveals the biomass of giant protists in the global ocean. Nature **532**: 504–507. doi:10.1038/nature17652

Bosse, A., and others. 2017. A submesoscale coherent vortex in the Ligurian Sea: From dynamical barriers to biological implications. J. Geophys. Res. Oceans **122**: 6196–6217. doi:10.1002/2016JC012634

Boucher, J. 1984. Localization of zooplankton populations in the Ligurian marine front: Role of ontogenic migration. Deep Sea Res A Oceanogr. Res Pap **31**: 469–484. doi:10.1016/0198-0149(84)90097-9

Boucher, J., F. Ibanez, and L. Prieur. 1987. Daily and seasonal variations in the spatial distribution of zooplankton populations in relation to the physical structure in the Ligurian Sea front. J. Mar. Res. **45**: 133–173. doi:10.1357/002224087788400891

Boyd, P., and P. Newton. 1995. Evidence of the potential influence of planktonic community structure on the interannual variability of particulate organic carbon flux. Deep Sea Res. I Oceanogr. Res. Pap. **42**: 619–639. doi:10.1016/0967-0637(95)00017-Z

Boyd, P. W., and P. P. Newton. 1999. Does planktonic community structure determine downward particulate organic carbon flux in different oceanic provinces? Deep Sea Res. I Oceanogr. Res. Pap. **46**: 63–91. doi:10.1016/S0967-0637(98)00066-1

Bruland, K. W., and M. W. Silver. 1981. Sinking rates of fecal pellets from gelatinous zooplankton (Salps, Pteropods, Doliolids). Mar. Biol. **63**: 295–300. doi:10.1007/BF00395999

Burd, A. B., and G. A. Jackson. 2009. Particle aggregation. Annu. Rev. Mar. Sci. **1**: 65–90. doi:10.1146/annurev.marine.010908.163904

Cowen, R. K., and C. M. Guigand. 2008. In situ ichthyoplankton imaging system (ISIIS): System design and preliminary results. Limnol. Oceanogr. Methods **6**: 126–132. doi:10.4319/lom.2008.6.126

Denman, K. L., and T. M. Powell. 1984. Effects of physical processes on planktonic ecosystems in the coastal ocean. Oceanogr. Mar. Biol. **22**: 125–168.

Dickey, T. D. 1991. The emergence of concurrent high-resolution physical and bio-optical measurements in the upper ocean and their applications. Rev. Geophys. **29**: 383–413. doi:10.1029/91RG00578

Dolan, J., and V. Raybaud. 2020. Zooplankton I. Micro- and mesozooplankton, p. 67–107. *In* The Mediterranean Sea in the era of global change 2. Wiley.

D'Ortenzio, F., and M. Ribera d'Alcalà. 2009. On the trophic regimes of the Mediterranean Sea: A satellite analysis. Biogeosciences **6**: 139–148. doi:10.5194/bg-6-139-2009

Faillettaz, R., M. Picheral, J. Y. Luo, C. Guigand, R. K. Cowen, and J.-O. Irisson. 2016. Imperfect automatic image classification successfully describes plankton distribution patterns. Methods Oceanogr. **15–16**: 60–77. doi:10.1016/J.MIO.2016.04.003

Ferrari, R. 2011. A frontal challenge for climate models. Science **332**: 316–317. doi:10.1126/science.1203632

Gasser, B., G. Payet, J. Sardou, and P. Nival. 1998. Community structure of mesopelagic copepods (>500 μm) in the Ligurian Sea (Western Mediterranean). J. Mar. Syst. **15**: 511–522. doi:10.1016/S0924-7963(97)00094-8

Goffart, A., J.-H. Hecq, and L. Prieur. 1995. Contrôle du phytoplancton du bassin ligure par le front liguro-provençal (secteur corse). Oceanol. Acta. **18**: 329–342.

Gorsky, G., N. L. da Silva, S. Dallot, P. Laval, J. C. Braconnot, and L. Prieur. 1991. Midwater tunicates: Are they related to the permanent front of the Ligurian Sea (NW Mediterranean)? Mar. Ecol. Prog. Ser. **74**: 195–204.

Gorsky, G., M. Picheral, and L. Stemmann. 2000. Use of the underwater video profiler for the study of aggregate dynamics in the North Mediterranean. Estuar. Coast. Shelf Sci. **50**: 121–128. doi:10.1006/ecss.1999.0539

Gorsky, G., L. Prieur, I. Taupier-Letage, L. Stemmann, and M. Picheral. 2002. Large particulate matter in the Western Mediterranean: I. LPM distribution related to mesoscale hydrodynamics. J. Mar. Syst. **33–34**: 289–311. doi:10.1016/S0924-7963(02)00063-5

Graham, W. M., F. Pagès, and W. M. Hamner. 2001. A physical context for gelatinous zooplankton aggregations: A review. Hydrobiologia **451**: 199–212. doi:10.1023/A:1011876004427

Greer, A. T., R. K. Cowen, C. M. Guigand, M. A. McManus, J. C. Sevadjian, and A. H. V. Timmerman. 2013. Relationships between phytoplankton thin layers and the fine-scale vertical distributions of two trophic levels of zooplankton. J. Plankton Res. **35**: 939–956. doi:10.1093/plankt/fbt056

Greer, A. T., R. K. Cowen, C. M. Guigand, and J. A. Hare. 2015. Fine-scale planktonic habitat partitioning at a shelf-slope front revealed by a high-resolution imaging system. J. Mar. Syst. **142**: 111–125. doi:10.1016/j.jmarsys.2014.10.008

Guidi, L., L. Stemmann, G. A. Jackson, F. Ibanez, H. Claustre, L. Legendre, M. Picheral, and G. Gorskya. 2009. Effects of phytoplankton community on production, size, and export of large aggregates: A world-ocean analysis. Limnol. Oceanogr. **54**: 1951–1963. doi:10.4319/lo.2009.54.6.1951

Guidi, L., and others. 2016. Plankton networks driving carbon export in the oligotrophic ocean. Nature **532**: 465–470. doi:10.1038/nature16942

Haury, L. R., J. A. McGowan, and P. H. Wiebe. 1978. Patterns and processes in the time-space scales of plankton distributions, p. 277–327. *In* J. H. Steele [ed.], Spatial pattern in plankton communities. Springer US.

Hays, G. C., A. J. Richardson, and C. Robinson. 2005. Climate change and marine plankton. Trends Ecol. Evol. **20**: 337–344. doi:10.1016/J.TREE.2005.03.004

Heinrich, A. K. 1962. The life histories of plankton animals and seasonal cycles of plankton communities in the oceans. J. Cons. Int. Explor. Mer. **27**: 15–24.

Kiørboe, T. 2001. Formation and fate of marine snow: Small-scale processes with large-scale implications. Sci. Mar. **65**: 57–71. doi:10.3989/scimar.2001.65s257

Legendre, L., and S. Demers. 1984. Towards dynamic biological oceanography and limnology. Can. J. Fish. Aquat. Sci. **41**: 2–19. doi:10.1139/f84-001

Legendre, P., and L. Legendre. 2012. Numerical ecology. Elsevier.

Lévy, M., P. J. S. Franks, and K. S. Smith. 2018. The role of submesoscale currents in structuring marine ecosystems. Nat. Commun. **9**: 4758. doi:10.1038/s41467-018-07059-3

Leys, C., C. Ley, O. Klein, P. Bernard, and L. Licata. 2013. Detecting outliers: Do not use standard deviation around the mean, use absolute deviation around the median. J. Exp. Soc. Psychol. **49**: 764–766. doi:10.1016/j.jesp.2013.03.013

Licandro, P., F. Ibañez, and M. Etienne. 2006. Long-term fluctuations (1974–99) of the salps *Thalia democratica* and *Salpa fusiformis* in the northwestern Mediterranean Sea: Relationships with hydroclimatic variability. Limnol. Oceanogr. **51**: 1832–1848. doi:10.4319/lo.2006.51.4.1832

Licandro, P., and P. Icardi. 2009. Basin scale distribution of zooplankton in the Ligurian Sea (north-western Mediterranean) in late autumn. Hydrobiologia **617**: 17–40. doi:10.1007/s10750-008-9523-9

Lombard, F., and T. Kiørboe. 2010. Marine snow originating from appendicularian houses: Age-dependent settling characteristics. Deep Sea Res I Oceanogr. Res. Pap. **57**: 1304–1313. doi:10.1016/j.dsr.2010.06.008

Lombard, F., and others. 2019. Globally consistent quantitative observations of planktonic ecosystems. Front. Mar. Sci. **6**: 196. doi:10.3389/fmars.2019.00196

Luo, J. Y., B. Grassian, D. Tang, J.-O. Irisson, A. T. Greer, C. M. Guigand, S. McClatchie, and R. K. Cowen. 2014. Environmental drivers of the fine-scale distribution of a gelatinous zooplankton community across a mesoscale front. Mar. Ecol. Prog. Ser. **510**: 129–149. doi:10.3354/meps10908

Mars Brisbin, M., O. D. Brunner, M. M. Grossmann, and S. Mitarai. 2020. Paired high-throughput, in situ imaging and high-throughput sequencing illuminate acantharian abundance and vertical distribution. Limnol. Oceanogr. **65**: 2953–2965. doi:10.1002/lno.11567

Mayot, N., and others. 2017. Physical and biogeochemical controls of the phytoplankton blooms in North Western Mediterranean Sea: A multiplatform approach over a complete annual cycle (2012–2013 DEWEX experiment). J. Geophys. Res. Oceans **122**: 9999–10019. doi:10.1002/2016JC012052

Mayot, N., P. Nival, and M. Levy. 2020. Primary production in the Ligurian Sea, p. 139–164. *In* The Mediterranean Sea in the era of global change 1. Wiley.

McClatchie, S., and others. 2012. Resolution of fine biological structure including small narcomedusae across a front in the Southern California bight. J. Geophys. Res. Oceans. **117**: C4. doi:10.1029/2011JC007565

Ménard, F., S. Dallot, G. Thomas, and J. C. Braconnot. 1994. Temporal fluctuations of two Mediterranean salp populations from 1967 to 1990. Analysis of the influence of environmental variables using a Markov chain model. Mar. Ecol. Prog. Ser. **104**: 139–152.

Millot, C. 1999. Circulation in the Western Mediterranean Sea. J. Mar. Syst. **20**: 423–442. doi:10.1016/S0924-7963(98)00078-5

Molinero, J. C., F. Ibanez, S. Souissi, E. Bosc, and P. Nival. 2008. Surface patterns of zooplankton spatial variability detected by high frequency sampling in the NW Mediterranean. Role of density fronts. J. Mar. Syst. **69**: 271–282. doi:10.1016/j.jmarsys.2005.11.023

Niculescu-Mizil, A., and R. Caruana. 2005. Predicting good probabilities with supervised learning, p. 625–632. *In* Proceedings of the 22nd International Conference on Machine Learning. Association for Computing Machinery.

Niewiadomska, K., H. Claustre, L. Prieur, and F. d'Ortenzio. 2008. Submesoscale physical-biogeochemical coupling across the Ligurian current (northwestern Mediterranean) using a bio-optical glider. Limnol. Oceanogr. **53**: 2210–2225. doi:10.4319/lo.2008.53.5_part_2.2210

Nival, P., F. Lombard, J. Cuzin, J. Goy, and L. Stemmann. 2020. Zooplankton II. Macroplankton and long-term series, p. 109–146. *In* The Mediterranean Sea in the era of global change 2. Wiley.

Orenstein, E. C., and others. 2022. Machine learning techniques to characterize functional traits of plankton from image data. Limnology and Oceanography. **67**: 1647–1669. doi:10.1002/lno.12101

Owen, R. W. 1981. Fronts and eddies in the sea: Mechanisms, interactions and biological effects. Anal. Mar. Ecosyst. 197–233.

Pedrotti, M. L., and L. Fenaux. 1992. Dispersal of echinoderm larvae in a geographical area marked by upwelling (Ligurian Sea, NW Mediterranean). Mar. Ecol. Prog. Ser. **86**: 217–227.

Picheral, M., L. Guidi, L. Stemmann, D. M. Karl, G. Iddaoud, and G. Gorsky. 2010. The underwater vision profiler 5: An advanced instrument for high spatial resolution studies of particle size spectra and zooplankton. Limnol. Oceanogr. Methods **8**: 462–473. doi:10.4319/lom.2010.8.462

Picheral, M., S. Colin, and J.-O. Irisson. 2017. EcoTaxa, a tool for the taxonomic classification of images.

Picheral, M., and others. 2021. The underwater vision profiler 6: An imaging sensor of particle size spectra and plankton, for autonomous and cabled platforms. Limnol. Oceanogr. Methods. doi:10.1002/lom3.10475

Pinca, S., and S. Dallot. 1995. Meso- and macrozooplankton composition patterns related to hydrodynamic structures in the Ligurian Sea (Trophos-2 experiment, April–June 1986). Mar. Ecol. Prog. Ser. **126**: 49–65. doi:10.3354/meps126049

Piterbarg, L., V. Taillandier, and A. Griffa. 2014. Investigating frontal variability from repeated glider transects in the Ligurian Current (North West Mediterranean Sea). J. Mar. Syst. **129**: 381–395. doi:10.1016/j.jmarsys.2013.08.003

Prieur, L., F. D'ortenzio, V. Taillandier, and P. Testor. 2020. Physical oceanography of the Ligurian Sea, p. 49–78. *In* The Mediterranean Sea in the era of global change 1. Wiley.

Remsen, A., T. L. Hopkins, and S. Samson. 2004. What you see is not what you catch: A comparison of concurrently collected net, optical plankton counter, and shadowed image particle profiling evaluation recorder data from the northeast Gulf of Mexico. Deep Sea Res. I Oceanogr. Res. Pap. **51**: 129–151. doi:10.1016/J.DSR.2003.09.008

Romagnan, J.-B., and others. 2015. Comprehensive model of annual plankton succession based on the whole-plankton time series approach. PLoS One **10**: e0119219. doi:10.1371/journal.pone.0119219

Rudnick, D. L., R. E. Davis, C. C. Eriksen, D. M. Fratantoni, and M. J. Perry. 2004. Underwater gliders for ocean research. Mar. Technol. Soc. J. **38**: 73–84. doi:10.4031/002533204787522703

Sandler, M., A. Howard, M. Zhu, A. Zhmoginov, and L.-C. Chen. 2019. MobileNetV2: Inverted residuals and linear bottlenecks. arXiv:1801.04381 [cs].

Sato, R., Y. Tanaka, and T. Ishimaru. 2003. Species-specific house productivity of appendicularians. Mar. Ecol. Prog. Ser. **259**: 163–172. doi:10.3354/meps259163

Schröder, S.-M., R. Kiko, and R. Koch. 2020. MorphoCluster: Efficient annotation of plankton images by clustering. Sensors **20**: 3060. doi:10.3390/s20113060

Steinberg, D. K., and M. R. Landry. 2017. Zooplankton and the ocean carbon cycle. Ann. Rev. Mar. Sci. **9**: 413–444.

Stemmann, L., G. Gorsky, J.-C. Marty, M. Picheral, and J.-C. Miquel. 2002. Four-year study of large-particle vertical distribution (0–1000 m) in the NW Mediterranean in relation to hydrology, phytoplankton, and vertical flux. Deep Sea Res II Top. Stud. Oceanogr. **49**: 2143–2162. doi:10.1016/S0967-0645(02)00032-2

Stemmann, L., L. Prieur, L. Legendre, I. Taupier-Letage, M. Picheral, L. Guidi, and G. Gorsky. 2008. Effects of frontal processes on marine aggregate dynamics and fluxes: An interannual study in a permanent geostrophic front (NW Mediterranean). J. Mar. Syst. **70**: 1–20. doi:10.1016/j.jmarsys.2007.02.014

Thyssen, M., and others. 2014. Onset of the spring bloom in the northwestern Mediterranean Sea: Influence of environmental pulse events on the in situ hourly-scale dynamics of the phytoplankton community structure. Front. Microbiol. **5**: 387.

Trudnowska, E., L. Lacour, M. Ardyna, A. Rogge, J. O. Irisson, A. M. Waite, M. Babin, and L. Stemmann. 2021. Marine snow morphology illuminates the evolution of phytoplankton blooms and determines their subsequent vertical export. Nat. Commun. **12**: 2816. doi:10.1038/s41467-021-22994-4

Turner, J. T. 2015. Zooplankton fecal pellets, marine snow, phytodetritus and the ocean's biological pump. Prog. Oceanogr. **130**: 205–248. doi:10.1016/J.POCEAN.2014.08.005

Vilgrain, L., F. Maps, M. Picheral, M. Babin, C. Aubry, J.-O. Irisson, and S.-D. Ayata. 2021. Trait-based approach using

in situ copepod images reveals contrasting ecological patterns across an Arctic ice melt zone. Limnol. Oceanogr. **66**: 1155–1167. doi:10.1002/lno.11672

Winder, M., and J. E. Cloern. 2010. The annual cycles of phytoplankton biomass. Philos. Trans. R. Soc. B Biol. Sci. **365**: 3215–3226. doi:10.1098/rstb.2010.0125

Acknowledgments

We thank the Alseamar Team and on duty pilots who supported us for glider piloting: Laurent Beguery, Florent Besson, Nicolas Buisson, David Diaz, Orens de Fommervault, and Marion Mery. The authors also thanks everyone who contributed to glider deployment or retrieval: Ewen Ancel, Marin Cornec, Paul Dasi, Florent Hallal, Gregory Maggion, Stéphane Renouf, Florian Ricour, Vincenzo Vellucci, and Laure Vilgrain. We thank the EMBRC platform PIQv for image analysis: this work was supported by EMBRC-France, whose French state funds are managed by the ANR within the Investments of the Future program under reference ANR-10-INBS-02. This study is part of the project "World Wide Web of Plankton Image Curation," funded by the Belmont Forum through the Agence Nationale de la Recherche ANR-18-BELM-0003-01. T,P.'s doctoral fellowship was granted by the French Ministry of Higher Education, Research and Innovation (3500/2019). T.P. also acknowledges Fabien Lombard and Lars Stemmann for the insightful discussions regarding the interpretation of observations, as well as Martin Schröder and Rainer Kiko for their assistance to accelerate the sorting plankton images with the Morphocluster application. This study has been conducted using E.U. Copernicus Marine Service Information (DOI: 10.48670/moi-00281).

Conflict of Interest

None declared.

Submitted 18 July 2023
Revised 19 January 2024
Accepted 21 March 2024

Guest editor: Heidi Sosik